View metadata, citation and similar papers at core.ac.uk
brought to you by CORE
provided by Open Archive Toulouse Archive Ouverte

# Chromium-based coatings by atmospheric chemical vapor deposition at low temperature from $Cr(CO)_6$

**Aurélia Douard and Francis Maury**

Centre Interuniversitaire de Recherche et d'Ingénierie des Matériaux (CIRIMAT), CNRS-INPT, ENSIACET, 118 Route de Narbonne 31077 cedex 4, France

## Abstract

Cr-based coatings were grown under atmospheric pressure in different gaseous atmospheres ($N_2$, $H_2$, $NH_3$) from the thermal decomposition of $Cr(CO)_6$ at 300 °C in a cold-wall CVD reactor. $Cr(CO)_6$ is a good candidate as precursor because of its low cost and its high volatility, which permits high flow rates.

Original chromium oxycarbide and oxynitride coatings were deposited on steel. These phases were previously obtained by plasma-assisted CVD and low-pressure CVD, i.e., under non-equilibrium conditions. In the present work, the low deposition temperature likely accounts for their formation. We have investigated correlations between the growth conditions and their main chemical, structural and physical features. Preliminary results on the mechanical behavior of these Cr-based coatings are also reported.

**Keywords:** MOCVD; Atmospheric deposition process; Chromium-based coatings; Chromium hexacarbonyl

1. Introduction
2. Experimental details
3. Results and discussion
3.1. Structural and chemical characterizations
3.1.1. Growth under N2 atmosphere
3.1.2. Growth under H2 atmosphere
3.1.3. Growth under NH3 gaseous atmosphere
3.2. Thermal stability of the coatings
3.2.1. Chromium oxycarbide coatings
3.2.2. Chromium oxynitride coatings
3.3. Preliminary adhesion properties
4. Conclusion
References

## 1. Introduction

Nowadays, metallurgical factories must combine productivity gain and production costs. Most metallurgical coatings are deposited using batch processes. For instance, vacuum processing requires stop periods, entailing servicing costs and productivity drop. That is why atmospheric processes are promising to answer industrial metallurgy needs. Atmospheric pressure chemical

vapor deposition (APCVD) is an attractive process for on-line strip coatings on metal pieces. Moreover, in chemical vapor deposition, the use of metallo-organic compounds as molecular precursors significantly decreases the deposition temperature. Combining both advantages, atmospheric MOCVD processes can find new industrial applications for the growth of metallurgical coatings.

Cr-based coatings are good candidates for the steel protection, owing to their good resistance to wear and corrosion and their high hardness. Coatings in the Cr–C–N system were previously reported by MOCVD operating generally under low pressure [1], [2] and [3]. $Cr(CO)_6$ is a good MOCVD precursor because it can be transported with a relatively high flow rate under atmospheric pressure, and it decomposes at low temperature. $Cr(CO)_6$ is stable under air protected from the light and must be handled cautiously, while its toxicological properties have not been fully investigated. Its homologues $W(CO)_6$ and $Mo(CO)_6$ were used in CVD processes operating under low pressure [4] and [5]. Chromium oxycarbides were first obtained by Lux et al. using $Cr(CO)_6$ [6]. The properties of $CrC_xO_y$ coatings obtained by low-pressure MOCVD [7], [8] and [9] and PVD [10] and [11] were studied. On the other hand, chromium oxynitride were only deposited by PVD [12] and [13] and the properties of these coatings have not been thoroughly investigated.

In this paper, $CrC_xO_y$, $CrO_y$ and $CrN_xO_y$ coatings were deposited under atmospheric pressure by MOCVD using $Cr(CO)_6$ as Cr-source and different reactive atmospheres. Thermal stability of these original phases are studied. Preliminary results on the adherence on 304L stainless steel of these Cr-based coatings are reported.

## 2. Experimental details

304L-type stainless steel small plates ($1 \times 1 \times 0.05$ cm$^3$) and Si(100) wafer ($1 \times 1$ cm$^2$) were used as substrates. Stainless steel substrates were mechanically mirror-like polished with SiC paper down to 4000 grade, then cleaned with acetone and ethanol in an ultrasonic bath. Si substrates were degreased in boiling tetrachloroethylene and boiling acetone, then rinsed in isopropanol. After cleaning, the substrates were dried under Ar stream and rapidly put into the reactor under vacuum ($10^{-4}$ Torr).

A vertical CVD Pyrex glass reactor was used. The substrates were supported by a SiC-passive graphite susceptor heated by HF induction. After 24 h pumping, the cold-wall CVD reactor was pressurized with nitrogen to 1 atm. The gas streams ($N_2$, $H_2$ and $NH_3$) were monitored using mass flow controllers and the total flow rate $D_T$ was maintained constant at 5000 cm$^3$/min, by adjusting the flow rates of carrier gas ($N_2$ or $H_2$), the dilution gas ($N_2$) and the reactive gas ($H_2$, $NH_3$). The $Cr(CO)_6$ powder used as precursor was placed in a thermostated saturator (60 °C) [14], in order to control its vapor pressure [15] and subsequently its flow rate. The precursor was transported in the gas phase to the reactor using either $N_2$ or $H_2$ stream.

The structure of the thin films was determined by X-ray diffraction (Cu Kα). The average crystallite size was determined using the Scherrer's formula from the width of the peak of the fcc structure of the deposited film. The chemical composition was analyzed by electron probe microanalysis (EPMA) and the surface morphology was examined by SEM. The chemical environment of the elements constituting the coatings was investigated by X-ray photoelectron spectroscopy (XPS) using a Mg X-ray source. To investigate their thermal stability, thin films grown on Si were sealed off under vacuum in quartz ampoules and annealed for 5 h at 500 °C, then additional 5 h at 650 °C. Adhesion of the coatings on stainless steel substrates was

characterized using a scratch tester (Revetest, CSM Instrument) with a Rockwell indenter ($R$ = 200 μm). The coatings were scratched under a normal increasing force of 10 N/min.

Table 1 summarizes the experimental runs and the main results of the structural and chemical characterizations of typical samples.

Table 1.

MOCVD conditions and principal characteristics of the $CrC_xO_y$, $CrO_y$ and $CrN_xO_y$ coatings grown using $Cr(CO)_6$ as precursor under atmospheric pressure

| Run | Growth conditions | | | | | Growth rate (μm/h) | Structure | Composition |
|---|---|---|---|---|---|---|---|---|
| | **Temperature (°C)** | **Gaseous atmosphere** | $x_R/x_P$ | $x_P$[a] (ppm) | $x_R$[b] (ppm) | | **XRD** | **EPMA** |
| 1 | 285 | $N_2$ | 0 | 338 | 0 | 1.9 | fcc CrCO | $Cr_{0.54}C_{0.21}O_{0.25}$ |
| 2 | 285 | $N_2$ | 0 | 100 | 0 | 1.2 | fcc CrCO | $Cr_{0.58}C_{0.16}O_{0.26}$ |
| 3 | 285 | $H_2$[c] | 1230 | 49 | 60,000 | 0.28 | fcc CrCO | $Cr_{0.45}O_{0.42}C_{0.13}$ |
| 4 | 285 | $H_2$ | 2010 | 30 | 60,000 | 0.57 | amorphous | $Cr_{0.39}O_{0.59}C_{0.02}$ |
| 5 | 300 | $NH_3$ | 2170 | 28 | 60,000 | 0.38 | fcc CrNO | $Cr_{0.33}O_{0.32}N_{0.28}C_{0.07}$ |
| 6 | 300 | $NH_3$ | 583 | 48 | 28,000 | 0.32 | fcc CrNO | $Cr_{0.43}O_{0.32}N_{0.20}C_{0.05}$ |
| 7 | 300 | $NH_3$ | 226 | 36 | 7200 | 0.39 | fcc CrNO | $Cr_{0.42}O_{0.28}N_{0.25}C_{0.05}$ |
| 8 | 300 | $NH_3$ | 152 | 47 | 8200 | 0.24 | fcc CrNO | $Cr_{0.35}O_{0.27}N_{0.33}C_{0.05}$ |
| 9 | 300 | $NH_3$ | 125 | 274 | 34,000 | 0.62 | fcc CrNO | $Cr_{0.35}O_{0.43}N_{0.19}C_{0.03}$ |
| 10 | 285 | $NH_3$ | 245 | 239 | 58,400 | 0.87 | fcc CrNO | $Cr_{0.48}O_{0.11}N_{0.39}C_{0.02}$ |
| 11 | 285 | $NH_3$ | 490 | – | – | 0.34 | fcc CrNO | $Cr_{0.45}O_{0.13}N_{0.39}C_{0.03}$ |
| 12 | 285 | $NH_3$ | 650 | 106 | 68,600 | 0.68 | fcc CrNO | $Cr_{0.48}O_{0.06}N_{0.43}C_{0.03}$ |

[a] Precursor mole fraction.
[b] Mole fraction of reactive gas.
[c] $H_2$ directly used as carrier gas.

# 3. Results and discussion

## 3.1. Structural and chemical characterizations

### 3.1.1. Growth under $N_2$ atmosphere

The films obtained under inert atmosphere are chromium oxycarbides ($CrC_xO_y$). They exhibit a dull-gray appearance and a relativity high surface roughness. SEM micrographs reveal a rough, nodular and porous surface morphology, made up of cauliflower-like grains with an average size of a few micrometers (Fig. 1). The nodular growth is clearly observed on cross sections. The morphology of the coatings either on stainless steel or on silicon substrates is the same. The growth rate increases from 1.2 (run 2) to 1.9 μm/h (run 1) by increasing the precursor molar fraction ($x_P$). The film composition (runs 1 and 2) is close to $Cr_{0.50}O_{0.25}C_{0.25}$ in good agreement with the chemical composition of the $Cr_2CO$ ternary phase reported by Watson et al. [16]. The XRD patterns of these coatings are similar to those reported in Ref. [8] (Fig. 2). They exhibit an fcc NaCl-type structure where the O and C atoms are presumably distributed randomly in the octahedral sites [16]. As-deposited films exhibit a nanocrystalline structure with a 30-nm crystallite size. Related coatings were previously deposited by PACVD using $Cr(CO)_6$ [17].

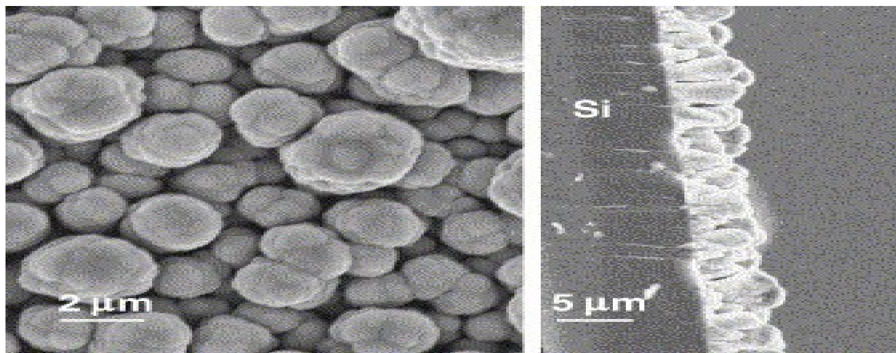


Fig. 1. Surface morphology and cross section of a $CrC_xO_y$ coating grown under $N_2$ atmosphere showing the nodular and cauliflower-like structure (run 1).

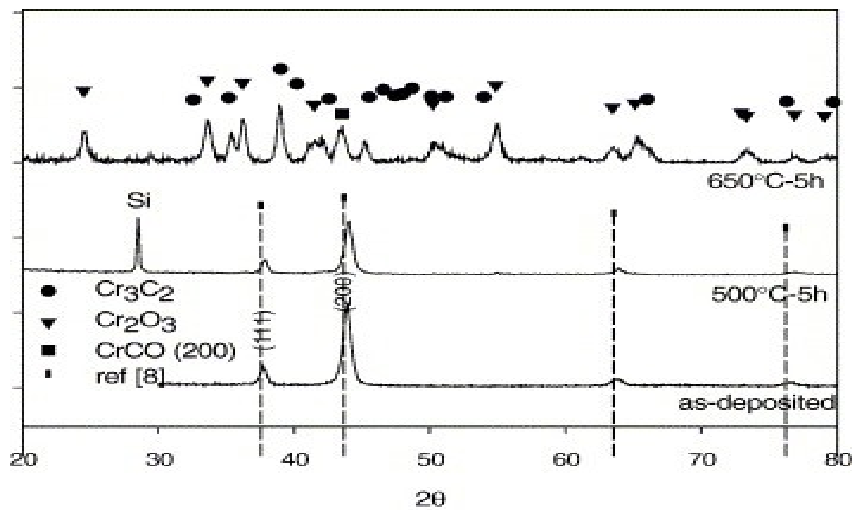


Fig. 2. XRD patterns of as-deposited and annealed $CrC_xO_y$ coatings grown on passivated Si(100) at 285 °C (run 1). The vertical dotted lines correspond to Ref. [8].

XPS spectra of as-deposited $CrC_xO_y$ films (run 1) after $Ar^+$ sputtering for the surface cleaning confirm the presence of Cr, C and O (Fig. 3). The film composition determined by XPS ($Cr_{0.49}O_{0.23}C_{0.28}$) is in good agreement with the EPMA data. The O 1s peak, found at 531.1 eV after sputtering, is characteristic of an oxide. The Cr $2p_{3/2}$ level is found at 576.6 eV on the surface spectrum and it shifts to 574.9 eV after removal of the surface contamination. There is no evidence of chromium metal, expected at 574.4 eV [18], but the Cr $2p_{3/2}$ peak could be consistent with a chromium carbide [19]. It has a nonsymmetrical shape with a carbide component at 574.9 eV and likely two oxide contributions at higher binding energy. The C 1s peak is also nonsymmetric on the high binding energy (Fig. 3) and it gives evidence for three carbon forms: the carbide which is dominant (282.8 eV), free or aliphatic carbon (285 eV) and C–O bonds (286.5 eV) [20]. In this cubic fcc structure, if C and O atoms are located in octahedral sites, they cannot be directly bonded. The presence of C–O bonds revealed by XPS proves that a small amount of O and/or C atoms are distributed in tetrahedral sites. There is no evidence for a polyphased structure constituted, for instance, by a mixture of carbide and oxide. The analyses indicate the formation of homogeneous chromium oxycarbide coatings.

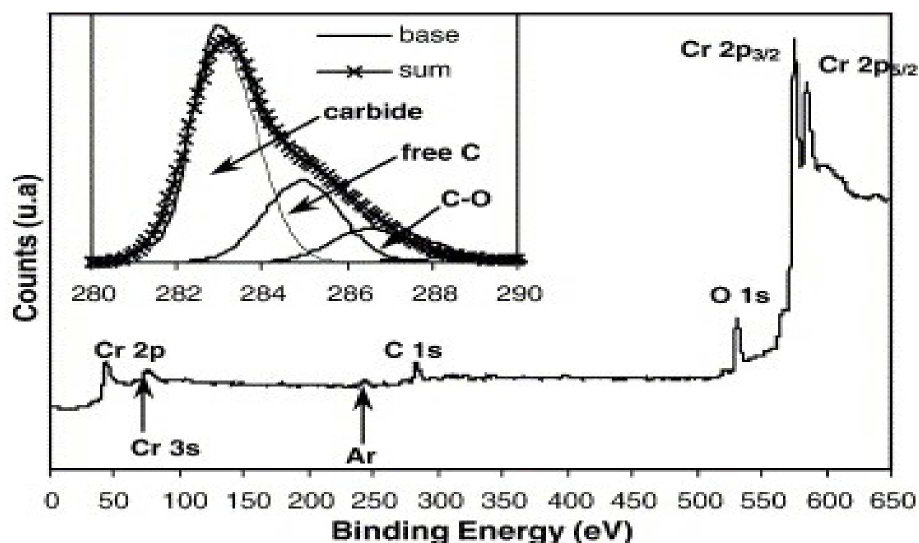


Fig. 3. Survey XPS spectrum of a $CrC_xO_y$ coating (run 1) and high-resolution area of C 1s peak after 20 min $Ar^+$ sputtering for the surface cleaning.

### 3.1.2. Growth under $H_2$ atmosphere

Depending on the carrier gas, two kinds of films were obtained (runs 3 and 4). When the precursor is transported using $N_2$ as carrier gas, and $H_2$ added at the entrance of the reactor (run 4), chromium oxides with almost negligible carbon content ($CrO_y$) are formed. They have a dark-gray appearance and a relative high surface roughness. Their morphology is similar to that of $CrC_xO_y$ obtained under $N_2$ atmosphere with a columnar structure, nodular grains with a mean size of 500 nm and a higher compactness (Fig. 4). The growth rate is 0.57 µm/h. The EPMA composition is $Cr_{0.39}O_{0.59}C_{0.02}$ that is almost the $Cr_2O_3$ stoichiometry. Clearly, increasing $H_2$ partial pressure decreases the C content up to negligible values (runs 2–4). However, by contrast with a previous claim, $H_2$ is not sufficient to completely reduce the coating and to form chromium metal [21]. The XRD pattern of run 4 shows an amorphous structure. The XPS spectra of $CrO_y$ coating (run 4) shows O 1s peak at 530.1 eV characteristic of an oxide and Cr $2p_{3/2}$ peak at 5726 eV, which is characteristic of $Cr_2O_3$, expected, for instance, around 576.8 eV [22]. After a few minutes of $Ar^+$ sputtering to clean the surface, no trace of C was found.

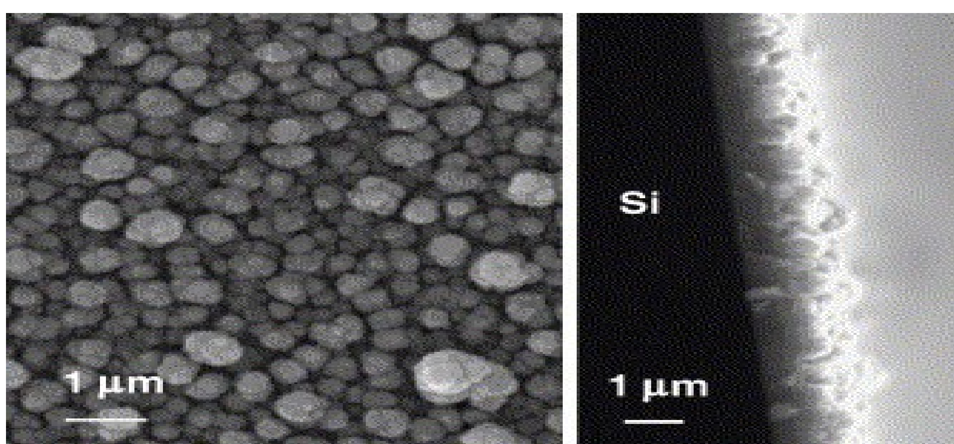


Fig. 4. Surface morphology and cross section of a $CrO_y$ coating grown under $H_2$ partial pressure (run 4).

In the particular case where $H_2$ is used both as carrier gas through the saturator and as reactive atmosphere in the reactor (run 3), a chromium oxycarbide is obtained instead of a chromium oxide. This coating exhibits a metallic brightness and dark gray color. A relatively smooth surface and a columnar growth with acicular grains of a few hundred nanometers long were observed. The typical growth rate is 0.28 µm/h. For these $CrC_xO_y$ coatings, the growth rate increases with the precursor mole fraction (run 1 and 2) and probably depends also on the partial pressure of additional reactive gas ($H_2$, $NH_3$). A discussion on the influence of these reactive gas requires further kinetic investigations. The EPMA composition is $Cr_{0.45}O_{0.42}C_{0.13}$ and the XRD pattern of run 3 is similar to runs 1 or 2. The cubic cell parameter calculated with the (200) peak is 0.408(3) nm while 0.412(3) nm was found for the $Cr_{0.54}O_{0.25}C_{0.21}$ composition (run 1) and 0.420 nm was previously reported for $Cr_{0.37}O_{0.21}C_{0.42}$ [11]. As a result, the cell parameter slightly increases with the C content. The XPS spectra are similar to those of run 1 and the deduced chemical composition is close to EPMA data. Under these CVD conditions, C is not completely removed. Probably, when $H_2$ is used as carrier gas, it reacts with $Cr(CO)_6$ and a premature decomposition occurs. Kado et al. noticed a different reactivity of the mixture $Cr(CO)_6/H_2$ depending on the

conditions of their PACVD process [17].

### 3.1.3. Growth under $NH_3$ gaseous atmosphere

The films obtained under $NH_3$ atmosphere are chromium oxynitride with a very low carbon content ($CrN_xO_y$). These samples have a metallic brightness and yellow-gray color. SEM micrographs show a fine-grained surface morphology, made up of small grains with a 100-nm mean size and a compact structure (Fig. 5). No difference was observed between the microstructure of the coatings grown either on silicon or on steel. The growth rate depends on the temperature, the precursor mole fraction and $NH_3$ partial pressure. It is close to 1 μm/h, but no attempt was made to optimize it. The C content is lower than 7 at.% and the N content is between 19 and 43 at.% (Table 1). Further experiments are required to discuss on the influence of the ratio $x_{NH3}/x_P$ and of the $NH_3$ mole fraction on the N content or on the growth rate. At this stage, we observe that $NH_3$ facilitates the carbon elimination from the coating to the gas phase, and for a fixed temperature and a given mole fraction of precursor (runs 5–8), it has no significant influence on the growth rate. These $CrN_xO_y$ coatings exhibit the same fcc structure as $CrC_xO_y$ (Fig. 6) but no data were found in the literature for chromium oxynitride. Interestingly, this structure is similar to that of CrN. As-deposited films have a nanocrystalline structure with a 30-nm crystallite size. The cell parameter is close to 0.412 nm (CrN: 0.414 nm), and no significant change was observed with the composition by contrast with the $CrC_xO_y$ films.

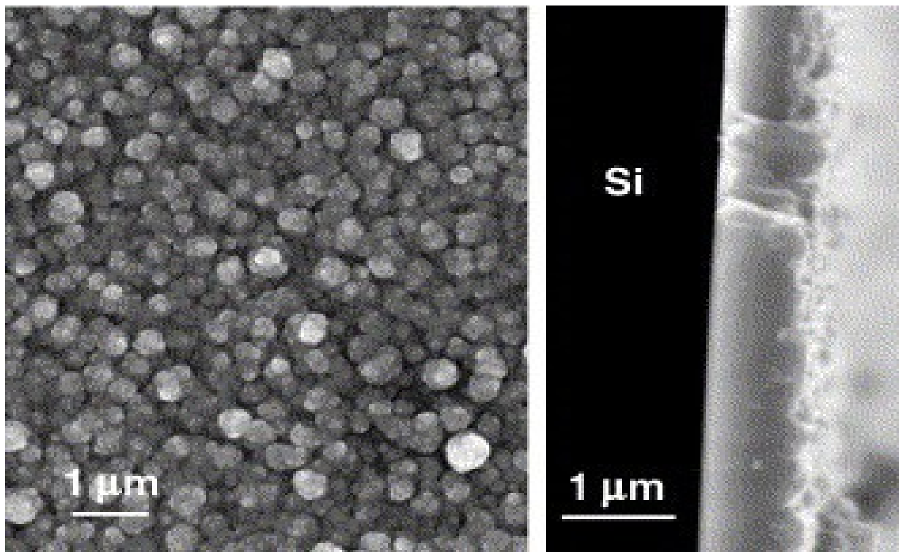


Fig. 5. Surface morphology and cross section of a $CrN_xO_y$ coating grown under $NH_3$ partial pressure (run 10).

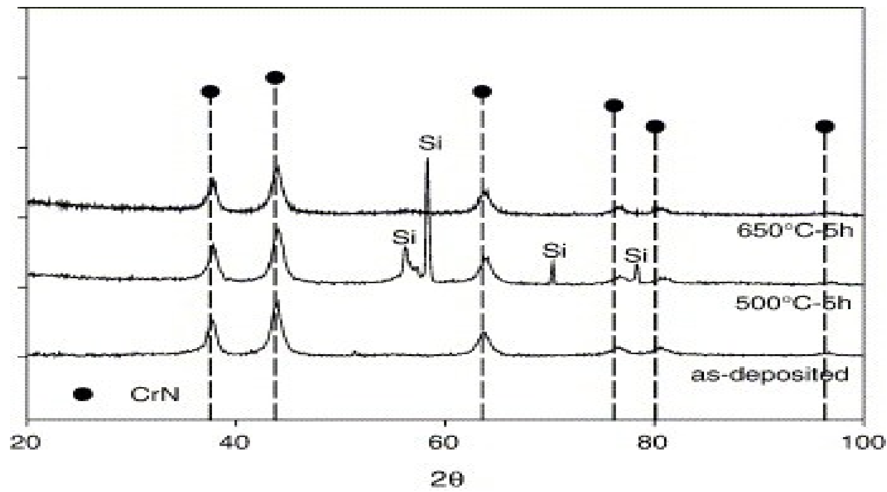


Fig. 6. XRD pattern of as-deposited and annealed $CrN_xO_y$ coatings grown at 300 °C on passivated Si(100) (run 8).

The XPS spectra of $CrN_xO_y$ coating (run 9) exhibit peaks for Cr, N and O and only traces of C after the surface cleaning by $Ar^+$ sputtering (Fig. 7). The XPS quantitative analysis ($Cr_{0.53}O_{0.35}N_{0.12}$) is close to the EPMA data ($Cr_{0.35}O_{0.43}N_{0.19}C_{0.03}$) for run 9. The Cr $2p_{3/2}$ level is found at 576.6 eV at the surface, and it shifts to 574.8 eV after $Ar^+$ sputtering to become dominant. This level is consistent with chromium nitride [23]. However, the FWHM of Cr $2p_{3/2}$ peak is broad (5eV), which denotes several components: Cr–N bonds and at least two chromium oxide contributions. The O 1s peak is found at 530.7 eV which is characteristic of an oxide. The N 1s peak is found at 397.4 eV, which is in the range of the nitrides: CrN 396.4 eV; $Cr_2N$ 397.2 eV [23]. Compared to the nitrides, the shift of Cr $2p_{3/2}$ and N 1s peak to the higher binding energies is due to the presence of oxygen which forms probably oxynitride bridges (Cr–N–O) [24]. Like the $CrC_xO_y$ phase, the existence of Cr–N–O bridges proves that few O and N atoms are also distributed in the tetrahedral sites. There is no evidence for a polyphased structure, and these coatings have to be considered as homogeneous chromium oxynitride.

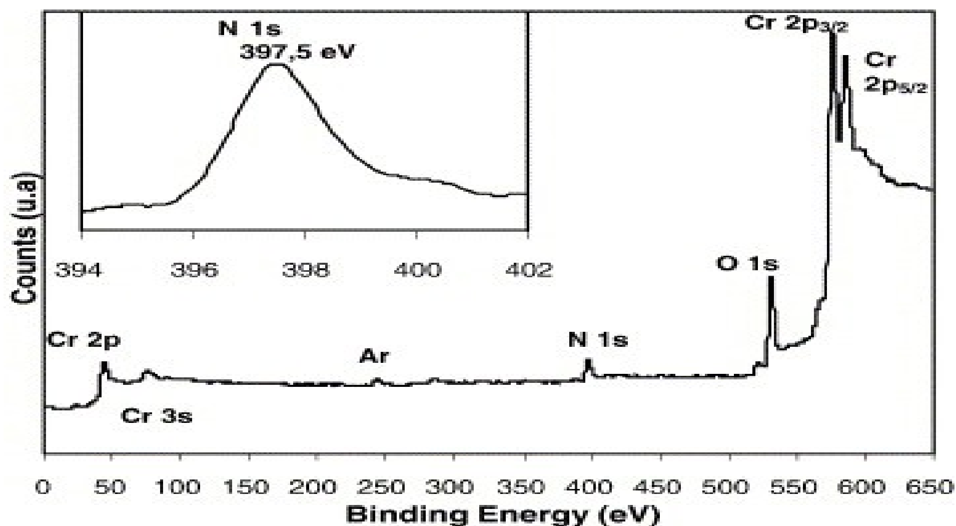


Fig. 7. Survey XPS spectrum of a $CrN_xO_y$ coating (run 9) and N 1s area spectrum after 20 min $Ar^+$ sputtering.

## 3.2. Thermal stability of the coatings

### 3.2.1. Chromium oxycarbide coatings

Good thermal stability is generally required for applications as protective metallurgical coatings. The literature reports several heat treatments of chromium oxycarbides [9] and [16] and chromium oxynitride [25]. This can be compared with our results. Fig. 2 shows the effect of annealing treatments on a representative $CrC_xO_y$ coating (run 1). This chromium oxycarbide sample was deposited at 285 °C and its structure is stable until 500 °C after 5 h (Fig. 2). At 650 °C, the formation of $Cr_2O_3$ and $Cr_3C_2$ occurs, but $CrC_xO_y$ is still present as evidenced by the (200) peak. Such a mixture of phases is not surprising because $Cr_2O_3$ and $Cr_3C_2$ are in thermodynamic equilibrium at high temperature [26]. When the C content is lower than the $Cr_2CO$ stoichiometry, as for the sample from run 3 ($Cr_{0.45}O_{0.42}C_{0.13}$), the coatings exhibit a lower thermal stability. For this coating, the formation of $Cr_2O_3$ starts at 500 °C, and there is no evidence for crystallized chromium carbides either at 500 °C or at 650 °C. In this case, upon the formation of $Cr_2O_3$, the C probably reacts with oxygen to produce $CO_2$ gas. The highest thermal stability of $CrC_xO_y$ is obtained for the film stoichiometry $Cr_2CO$.

When the growth occurs under a large excess of $H_2$ (run 4), an amorphous chromium oxide is deposited with a ratio O:Cr = 1.51 (Table 1). Surprisingly, after annealing for 5 h at 500 °C, it crystallizes with the fcc-structure rather than the structure of $Cr_2O_3$ (O:Cr = 1.50) although the C content was negligible. Chromium oxides with O:Cr = 1:1 and fcc-structure have already been reported in the literature [27]. After annealing at 650 °C for additional 5 h, evidence for amorphization is given by the broadening of the fcc peaks.

### 3.2.2. Chromium oxynitride coatings

No significant changes were observed in the XRD pattern of $CrN_xO_y$ coatings (run 8) after annealing at 650 °C (Fig. 6). The cell parameter does not change and the FWHM of the peak indicates that the nanocrystalline structure is maintained. These chromium oxynitride coatings exhibit a high thermal stability.

## 3.3. Preliminary adhesion properties

For the $CrC_xO_y$ sample (run 1; thickness = 4 μm), partial detachment of the coating started both inside and outside the scratch trace for a load of 4–7 N. Important decohesion was observed for a critical load ($LC_d$) of 16 N. For a $CrC_xO_y$ coating twice thinner (2 μm), the $LC_d$ value was significantly lower (8 N). There was a continuous ductile perforation of the coating and a complete removal for a critical load ($LC_u$) of 35 N for a 4-μm-thick coating and 22 N for a 2-μm-thick coating. These buckling and spallation failure modes are characteristic of poor adhesion. This is in agreement with the porous structure of these coatings (Fig. 1).

For $CrO_y$ film (run 4; 1.3 μm), interfacial spallation was observed at the edge and the bottom of the scratch track at $LC_d$ = 9 N. The coating was completely removed in the track at $LC_u$ = 24 N.

For $CrN_xO_y$ (run 10; 0.85 μm) interfacial spallation at the edge and the bottom of the scratch track was observed for $LC_d$ = 15 N. In the track, no coating was found after $LC_u$ = 35 N. Thinner

$CrN_xO_y$ coatings (run 9; 0.29 µm and run 11; 0.5 µm) exhibit a less pronounced degradation. For the 0.50-µm-thick coating, we found $LC_d$ = 18 N and $LC_u$ = 36 N, while for the 0.29-µm-thick coating, the values were $LC_d$ = 20 N and $LC_u$ = 42 N. The two types of critical loads and their difference are higher for thinner $CrN_xO_y$ coatings. As a result, thinner $CrN_xO_y$ seem to have a better adhesion than thick $CrN_xO_y$ coatings. It can be explained by their lower internal stresses compared to the thicker coatings.

## 4. Conclusion

Chromium oxycarbides $CrC_xO_y$, chromium oxides $CrO_y$ and chromium oxynitrides $CrN_xO_y$ were deposited by MOCVD under atmospheric pressure on stainless steel substrates, at temperatures as low as 300 °C using $Cr(CO)_6$ as Cr-source and with, respectively, $N_2$, $H_2$ and $NH_3$ as gaseous atmosphere. $CrC_xO_y$ and $CrN_xO_y$ thin films exhibit a nanocrystalline fcc structure while $CrO_y$ is amorphous. XRD and XPS characterizations of $CrC_xO_y$ and $CrN_xO_y$ gave evidence for single-phase coatings. The thermal stability of $CrC_xO_y$ depends of the C content and it is optimized for the $Cr_2CO$ stoichiometry. For this composition, $Cr_2O_3$ and $Cr_3C_2$ are formed after annealing at 650 °C. $CrC_xO_y$ thin films exhibit a nodular growth and a porous morphology, leading to poor mechanical properties. $CrN_xO_y$ coatings exhibit a smooth surface morphology and a compact structure. Some obtained chromium oxynitride compositions exhibit a Cr:N ratio close to 1:1, with a low content of oxygen and carbon. Furthermore, they are thermally stable above 650 °C. Preliminary adherence tests have revealed promising performances of $CrN_xO_y$ to be used as metallurgical protective coatings. Optimization of the growth process and further characterizations of the coatings are currently in progress.

## References


F. Schuster, F. Maury, J.F. Nowak and C. Bernard, *Surf. Coat. Technol.* 46 (1991), p. 275.

F. Schuster, F. Maury, N. Pébère, J.F. Nowak and C. Duret-Thual, *Innovation and Technology Transfer for Corrosion Control (Proceed 11th Int. Corrosion Congress)* vol. 1 (1990), p. 205.

F. Maury, F. Ossola and F. Senocq, *Surf. Coat. Technol.* 133–134 (2000), p. 198.

L.H. Kaplan and F.M. d'Heurle, *J. Electrochem. Soc.* 117 (1970) (5), p. 693.

B.H. Lee and K. Yong, *J. Electrochem. Soc.* 151 (2004) (9), p. C594.

H. Lux and A. Ignatowicz, *Chem. Ber.* 101 (1968), p. 809.

T. Kado and Y.J. Noda, *Jpn. J. Appl. Phys.* 28 (1989) (8), p. 1450.

M. Kmetz, B.J. Tan, W. Willis and S. Suib, *J. Mater. Sci.* 26 (1991), p. 2107.

T. Kado, *J. Am. Ceram. Soc.* 82 (1999) (11), p. 3245.

A.M. Peters, X.M. He, M. Trkula and M. Nastasi, *Nucl. Instrum. Methods Phys. Res., B* 175–177 (2001), p. 599.

T. Kado and Q. Fan, *J. Am. Ceram. Soc.* 84 (2001) (8), p. 1763.

T. Suzuki, H. Saito, M. Hirai, H. Suemtsu, W. Jiang and K. Yatsui,*Thin Solid Films* 407 (2002), p. 118.

S. Agouram, F. Bodart and G. Terwagne, *Surf. Coat. Technol.* 180 (2004), p. 164.

A. Douard, F. Maury, Récents Progrès en Génie des Procédés, 82 (in press).

M. Manly, M. Windsor and A.A. Blanchard, *J. Am. Chem. Soc.* 56 (1934), p. 823.

I.M. Watson and J.A. Connor, *Polyhedron* 8 (1989) (13–14), p. 1794.

T. Kado and Y.J. Noda, *J. Electrochem. Soc.* 136 (1989) (8), p. 2184.

F. Maury, C. Vahlas, S. Abisset and L. Gueroudji, *J. Electrochem. Soc.* 146 (1999) (10), p. 3716.

F. Schuster and F. Maury, *Surf. Coat. Technol.* 43/44 (1990), p. 185.

D. Rats, L. Vandenbulcke, R. Herbin, R. Benoit, R. Erre, V. Serin and J. Sevely, *Thin Solid Films* 270 (1995), p. 177.

J.J. Lander and L.H. Germer, *Am. Inst. Min. Metall. Eng., Tech. Publ.* 2259 (1947 (Sept.)).

F.M. Capece, V. Dicastro, C. Furlani, G. Mattogno, C. Fragale, M. Gargano and M. Rossi, *J. Electron Spectrosc. Relat. Phenom.* 27 (1982), p. 119.

O. Nishimura, K. Yabe and M. Iwaki, *J. Electron Spectrosc. Relat. Phenom.* 49 (1989), p. 335.

I. Bertodi, M. Mohai, P.H. Mayrhorfer and C. Mitterer, *Surf. Interface Anal.* 34 (2002), p. 740.

M.P. Roubin and J.M. Pâris, *C. R. Acad. Sci. Paris* (1965 (5 Avril)), p. 3981 (t.260 groupe 8).

A.A. Popov, P.N. Ostrik and M.I. Gasik, *Izv. Vyss. Ucebn. Zaved., Chern. Metall.* 10 (1986), p. 1Cited By in Scopus (0)

V. Dufek, F. Petru and V. Brozek, *Monatsh. Chem.* 98 (1967), p. 2424.

**Original text : Elsevier.com**